

PAPER • OPEN ACCESS

## Effects of Cr addition on the microstructures and oxidation of Nb-Si-Al-Ti-W alloys

To cite this article: W Y Long and H M Jia 2019 *IOP Conf. Ser.: Mater. Sci. Eng.* **479** 012072

View the [article online](#) for updates and enhancements.



**IOP | ebooks™**

Bringing you innovative digital publishing with leading voices to create your essential collection of books in STEM research.

Start exploring the collection - download the first chapter of every title for free.

# Effects of Cr addition on the microstructures and oxidation of Nb-Si-Al-Ti-W alloys

W Y Long<sup>1</sup> and H M Jia

College of Aeronautical Manufacturing Engineering, Nanchang Hangkong University, Nanchang 330063, China

<sup>1</sup>E-mail: long\_weny@sohu.com

**Abstract.** The effects of Cr addition on the microstructures and oxidation kinetics of the Nb-20Si-5Al-15Ti-5W alloys have been investigated in this study. The alloys were prepared by Spark Plasma Sintering (SPS) technology. The results show that the microstructure of the alloys consists of (Nb, Ti, W)<sub>ss</sub>,  $\alpha$ -Nb<sub>5</sub>Si<sub>3</sub>,  $\gamma$ -Nb<sub>5</sub>Si<sub>3</sub> and (Nb, Ti)<sub>5</sub>Si<sub>3</sub> phase. The addition of 3at% Cr improves the oxidation resistance of the composite at 800°C and 1100°C dramatically. The AlNb<sub>11</sub>O<sub>29</sub>, Ti<sub>2</sub>Nb<sub>10</sub>O<sub>29</sub>, TiO<sub>2</sub>, Nb<sub>2</sub>O<sub>5</sub>, Cr<sub>2</sub>Ti<sub>6</sub>O<sub>15</sub>, and Nb<sub>4</sub>W<sub>3</sub>O<sub>47</sub> are present in the scales formed at 800°C. The phases present in the oxide scales formed at 1100°C consisted of AlNb<sub>11</sub>O<sub>29</sub>, Ti<sub>2</sub>Nb<sub>10</sub>O<sub>29</sub>, TiO<sub>2</sub>, Cr<sub>2</sub>WO<sub>6</sub>, and Nb<sub>2</sub>O<sub>5</sub>. The oxidation resistance of the composite at 1100°C is better than at 800°C because the oxide scale is more compact structure.

## 1. Introduction

In order to promote more advanced aerospace gas turbines and aircraft engines, the high temperature structural materials exhibiting excellent mechanical strength and creep resistance, good microstructure stability and oxidation resistance are essential. Nb-Si based in situ composites are considered attractive for possible replacement of Ni-base super alloys for high temperature (>1200°C) applications due to their higher melting point (>1750°C), lower density (6.6-7.2 g/cm<sup>3</sup>), good oxidation resistance and capacity to retain enough strength at and above 1200°C are desired [1]. However, their poor oxidation resistance at intermediate and high temperatures is still one of the major difficulties to their use in high temperature applications.

In recent years, many efforts have been devoted to looking for alloying elements and optimizing their content to enhance the oxidation behavior. The Nb-Si system has been developed to obtain the expected overall performance, while the Si content typically ranges from 12 to 25 at%. Previous work has shown that the mechanical property and the oxidation resistance of the Nb/Nb<sub>5</sub>Si<sub>3</sub> in situ composites can be improved significantly by alloying with Cr, Al, Ti, Mo, W, Ge, Sn, Ga, and Hf [2–20]. The Cr content affects the fracture toughness at room temperature [8] and the high-temperature oxidation resistance [9]. The oxidation-resisting Cr<sub>2</sub>Nb phases are typically introduced with higher content of Cr additions [5]. Unfortunately, the level of alloying required for the improvement of oxidation resistance could sacrifice the room temperature fracture toughness and high temperature strength of the composites. Therefore, further investigations are needed to achieve the required balance of oxidation performance and mechanical properties.



Therefore, the effect of Cr contents on the microstructures and oxidation resistance of the Nb-20Si-5Al-15Ti-5W alloys were studied in the present investigation. The alloys were fabricated by SPS technology. The results were believed to be of great importance for engineering application.

## 2. Experimental conditions and methods

The nominal compositions of the alloys were Nb-20Si-5Al-15Ti-5W(NC1), Nb-20Si-5Al-15Ti-5W-3Cr(NC2) and Nb- 20Si-5Al-15Ti-5W-5Cr (NC3) (in this paper all compositions are given in at.% unless stated otherwise). The alloys were prepared by SPS in a vacuum atmosphere. The powders were milled under argon atmosphere in the ball grinder for 24h, and the mixed powders were packed into a graphite die with an inside diameter of 20mm. The sintering was carried out on a SPS machine manufactured by Sumitomo Coal Mining Co. Ltd., Japan. A uniaxial load of 11kN was applied on the powders to realize sintering and densification simultaneously. A heating speed of 150°C/min and the sintering temperature of 1500°C were adopted under fixed sintering holding time of 10 min.

Samples (6mm×6mm×6mm) for the oxidation experiment were polished to 1500 grit SiC paper and cleaned in ethanol and acetone. The isothermal oxidation experiments were undertaken in a muffle furnace for 100h both at 800°C and 1100°C. The specimens were weighed by using a precision analytical balance (Model FA2004, China) with an accuracy of 0.01 mg. The microstructures of the specimen, coatings and oxidized scales were examined using a MeF-3 optical microscope and a JSMT-200 scanning electron microscope (SEM). X-ray diffraction (D/MAX-IIIB) patterns of the bulk specimens were obtained to identify the phases.

## 3. Results and Discussion

### 3.1. Microstructure and morphology of alloy

Figure 1 gives the XRD patterns of each composite studied in this work, where the dashed lines represent the diffraction peak positions of the pure Nb (JCPDS 34-370). It is obvious from Figure 1 that the peaks of Nbss and Nb<sub>5</sub>Si<sub>3</sub> are detected, but the peaks of Si, Al, Ti, W, Cr, and Nb<sub>3</sub>Si are not detected. It is readily seen in these diffractograms that the Nbss peaks in all the alloys were shifted slightly to the right (higher 2θ values) of the intensity peaks expected for pure niobium, which would suggest that the Nbss phase in each alloys has a reduced lattice parameter compared with pure niobium.

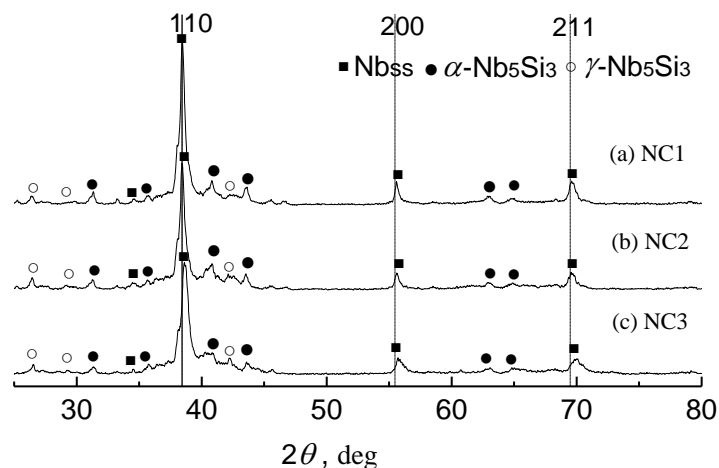


**Figure 1.** XRD patterns of the Nb-20Si-5Al-15Ti-5W alloys.

The lattice parameter  $a$  of the *bcc* Nbss was calculated using the relation  $a = d\sqrt{(h^2 + k^2 + l^2)}$ , where  $h$ ,  $k$ ,  $l$  are plane indices, and the Nelson-Riley extrapolation method [18]. The estimated lattice parameters of the *bcc* Nbss in the alloys are shown in Figure 2, where data of pure niobium (3.303 Å, JCPDS 34-370) are also given for comparison. Figure 3 shows that the lattice parameters of the Nbss in all the composites were smaller than that of the pure niobium. Since the atomic radii of the pure Nb,

Ti, Si, Al, W and Cr are 1.47, 1.47, 1.17, 1.43, 1.41 and 1.30 Å, respectively [21], the contracted Nbss lattice in these alloys is attributed to the substitutions of Ti, Al, Si and W for the larger Nb atom in the solid solution, considering only the size effect of substitutional atoms for Nb. The same result is also found in other work on Nb-Si based alloys [18]. The lattice parameter of the Nbss in NC1 was 3.296 Å (Figure 2), which is about 0.2% smaller than of pure Nb. Furthermore the lattice parameters decreased with increasing Cr concentration.

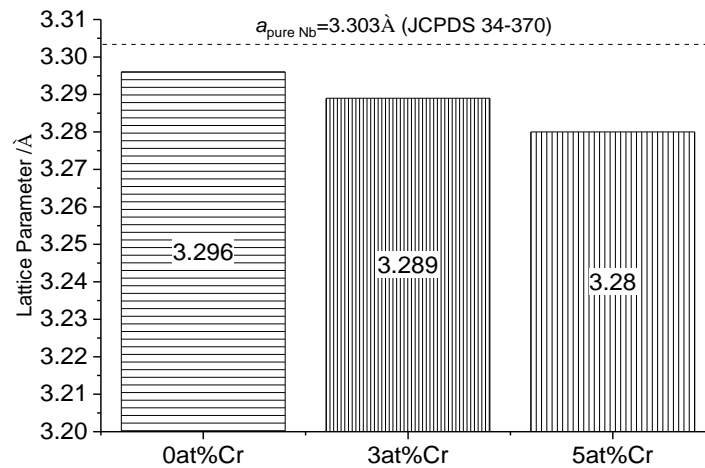


**Figure 2.** The lattice parameters of the *bcc* Nbss in the alloys.

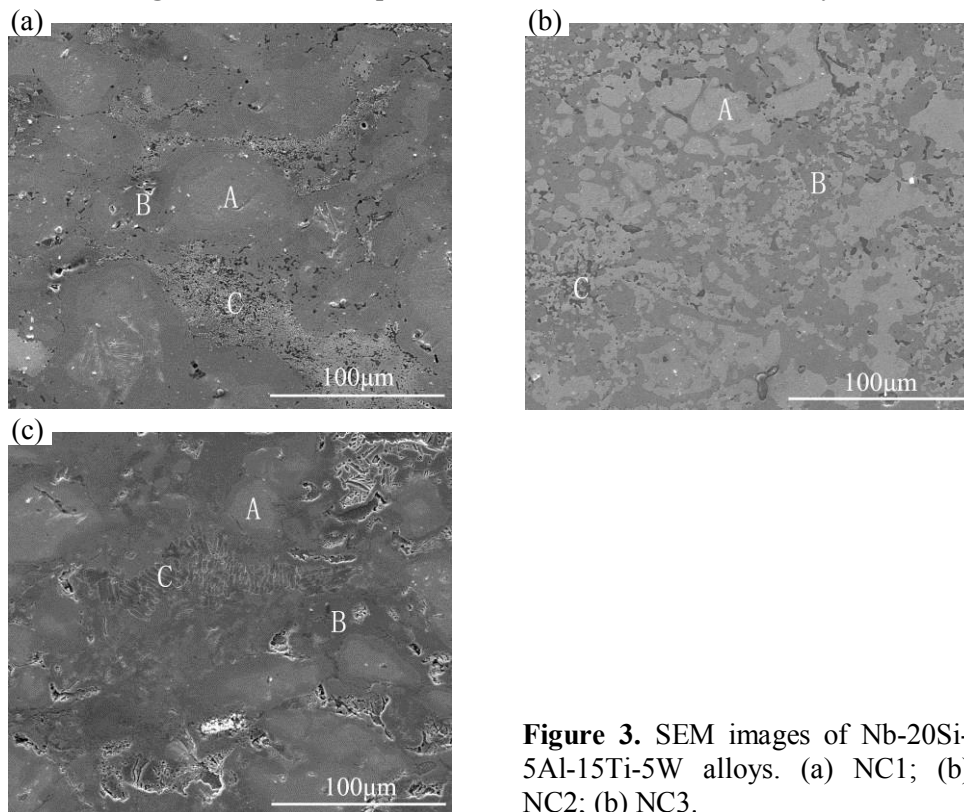


**Figure 3.** SEM images of Nb-20Si-5Al-15Ti-5W alloys. (a) NC1; (b) NC2; (c) NC3.

Figure 3 shows the SEM image of Nb/Nb<sub>5</sub>Si<sub>3</sub> composite prepared via SPS. The microstructure consisted of the Nbss and Nb<sub>5</sub>Si<sub>3</sub>. These phases exhibit light and dark contrast, respectively, in Figure 3. It is evident that the effects of Cr on the microstructure of Nb/Nb<sub>5</sub>Si<sub>3</sub> alloys are inconspicuous and the microstructure is not changed. The bright particle phase in Figure 3(a) (point A) contains Nb, Al,

and Ti, and the black particle phase in Figure 3(a) (point C) contains Nb, and Ti, whereas the dark matrix (point B) contains both Nb, Si Al, and Ti. Figure 3(b) and (c) show that point A contains Nb, point B and point C contain Nb, Si, Ti, and W. Therefore the alloys comprised of Nb<sub>SS</sub> and Nb<sub>5</sub>Si<sub>3</sub>, and Ti, W and Al are solubilized in Nb<sub>SS</sub> and Nb<sub>5</sub>Si<sub>3</sub> phases respectively.

### 3.2. Oxidation kinetics

The oxidation rates of the alloys were measured at 800°C and 1100°C in static air. The thermogravimetric results are shown in Figure 4, in which the weight change (g/cm<sup>2</sup>) is plotted as a function of oxidation time (h). The isothermal oxidation tests showed that the weight changes of NC1 and NC3 followed parabolic oxidation kinetics while that of NC2 was linear at 800°C. The oxidation kinetics of NC1, NC2 and NC3 were linear at 1100°C.

With an increase of Cr addition, the oxidation resistance of the composite at 800°C increases firstly and then decreases. Therefore the NC3 alloy which exhibited the highest weight gain, showed very poor oxidation behaviour at 800°C. The weight gain of NC3 was 190mg/cm<sup>2</sup> after 22h at 800°C, then changed little over time. It was suggested that the rectangular NC3 sample had completely disintegrated into powder when exposed to air for ~22h. The NC1 exhibited the worse oxidation behavior among the other alloy, and the weight gain was 143mg/cm<sup>2</sup> after 22h at 800°C, then the oxidation rate increased resulting in a weight gain of 259mg/cm<sup>2</sup> after 100h. In the presence of 3 at% Cr, the NC2 composite showed the lowest weight gain rate, and the weight gain was 148mg/cm<sup>2</sup> after 100h at 800°C.

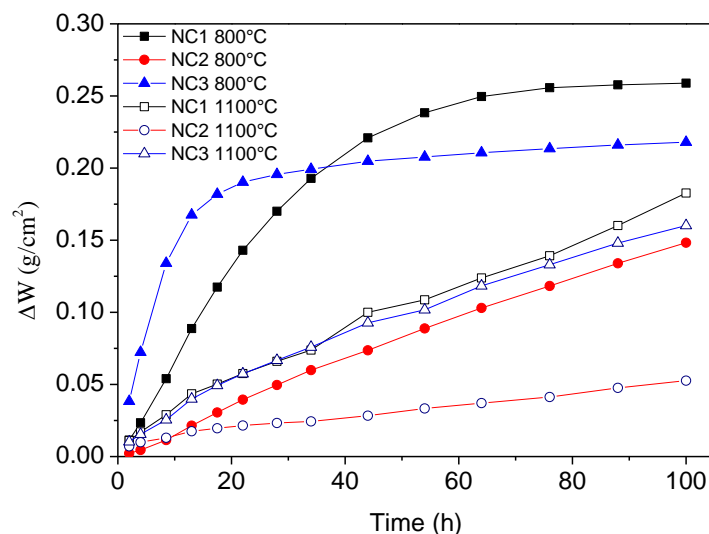


**Figure 4.** Weight gain curve of sample at 800°C and 1100°C.

The sample is not completely oxidized after being exposed to air for 100 h at 1100 °C. The high-temperature antioxidation of the Nb-Si alloy without alloying is very poor. The high-temperature oxidation resistance is improved by multi-element alloying, particularly at 1100°C, which is better than that at 800°C. As seen in Figure4, after 100h exposure to air at 1100°C the weight gains of the NC1, NC2 and NC3 were 183, 52.6 and 160 mg/cm<sup>2</sup>, respectively. The alloys were not completely oxidized after so many hours.

### 3.3. Morphology and composition of the oxide scale

A SEM image of sample oxide scale is presented in Figure 5 and Figure 6. The XRD patterns of the oxide scale on the samples are presented in Figure 7.

According to the XRD data (Figure 7a), the oxides formed on the NC1 sample are mainly AlNb<sub>11</sub>O<sub>29</sub>, Ti<sub>2</sub>Nb<sub>10</sub>O<sub>29</sub>, TiO<sub>2</sub>, Nb<sub>2</sub>O<sub>5</sub> and Nb<sub>4</sub>W<sub>13</sub>O<sub>47</sub>. The peak intensity of Nb<sub>2</sub>O<sub>5</sub> diffraction is the

strongest. It is suggested that the oxidation product is dominated by  $\text{Nb}_2\text{O}_5$  at  $800^\circ\text{C}$ . The molar volume of Nb is  $10.9\text{cm}^3$ , but that of  $\text{Nb}_2\text{O}_5$  is  $58.3\text{cm}^3$ . The formation of  $\text{Nb}_2\text{O}_5$  from Nbss phases normally introduces significant volume expansion up to 169%, and the generation of large residual stress in the oxide scales resultantly [22, 23]. The oxides scales formed on Nb-Si based alloys are typically porous and less protective, and have a high tendency of spallation during oxidation. The oxygen can easily diffuse in the  $\text{Nb}_2\text{O}_5$  scale and Nb undergoes rapidly pest oxidation. The continuous absorption, dissolution and inward diffusion of oxygen are typically through Nbss phases, in which the solubility of oxygen is higher and the diffusion rate of oxygen is faster [24]. Thus it is the key to enhance the oxidation resistance of Nb-Si alloys by improving the anti-oxidation ability of Nbss phases.

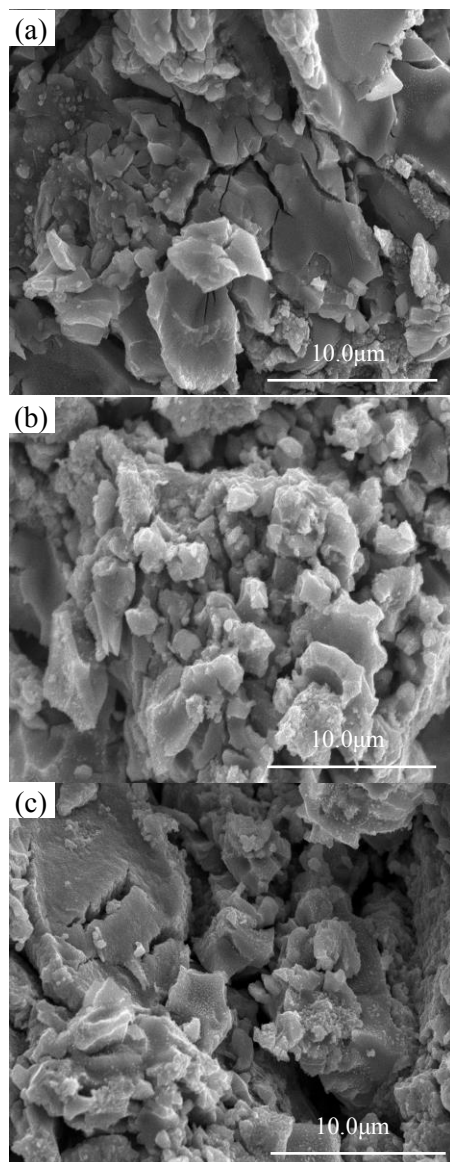


**Figure 5.** SEM photographs of sample oxide scale after oxidation at  $800^\circ\text{C}/100$  h. (a) NC1; (b) NC2; (c) NC3.

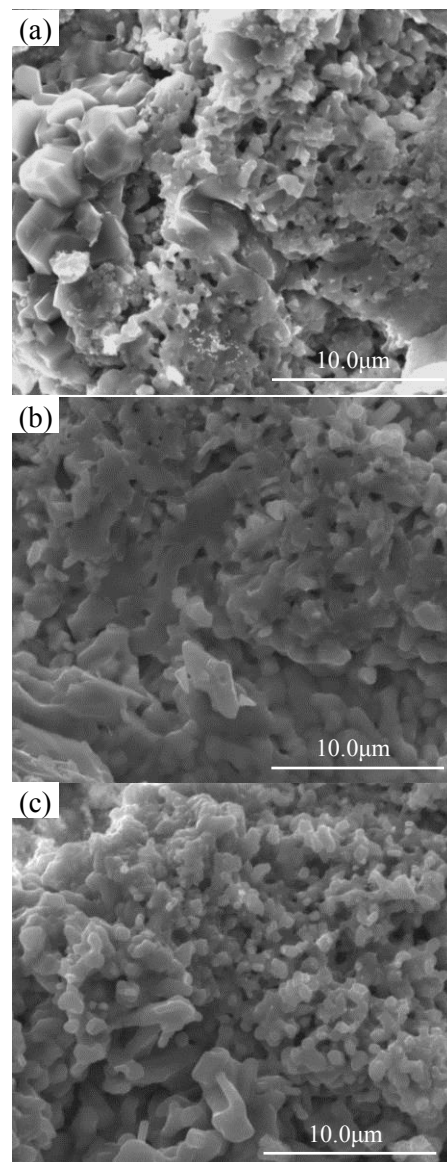


**Figure 6.** SEM photographs of sample oxide scale after oxidation at  $1100^\circ\text{C}/100$  h. (a) NC1; (b) NC2; (c) NC3.

With the addition of Cr, the  $\text{CrNbO}_4$  was present in the oxidized NC2 and NC3 as shown in Figures 7(b) and (c), which are expected to be the oxidation resistant oxides. The intensity of the XRD pattern for  $\text{CrNbO}_4$  occurs at  $2\theta = 27.3^\circ$ , while those for  $\text{Nb}_2\text{O}_5$  occur at  $2\theta = 23.9^\circ$ . The ratio of the intensity,  $I_{\text{CrNbO}_4}$ , of the  $\text{CrNbO}_4$  peak at  $2\theta = 27.3^\circ$  to the intensity,  $I_{\text{Nb}_2\text{O}_5}$ , at  $2\theta = 23.9^\circ$  can be used as a measure of the relative amounts of  $\text{CrNbO}_4$  and  $\text{Nb}_2\text{O}_5$  in the oxidation products [25]. It could be found that the ratio of NC2 is higher than that of NC3. For NC1 and NC3, the oxide scale peels off continuously during oxidation due to the larger volume of  $\text{Nb}_2\text{O}_5$ , resulting in the loose and micro crack oxide scales (as shown in Figure 5a and 5c). For NC2 alloy, the solid state reaction occurs completely as its oxide scale adhered on the substrate during the oxidation (as shown in Figure 5b). Therefore, the oxidation resistance of NC2 is better than that of NC1 and NC3.

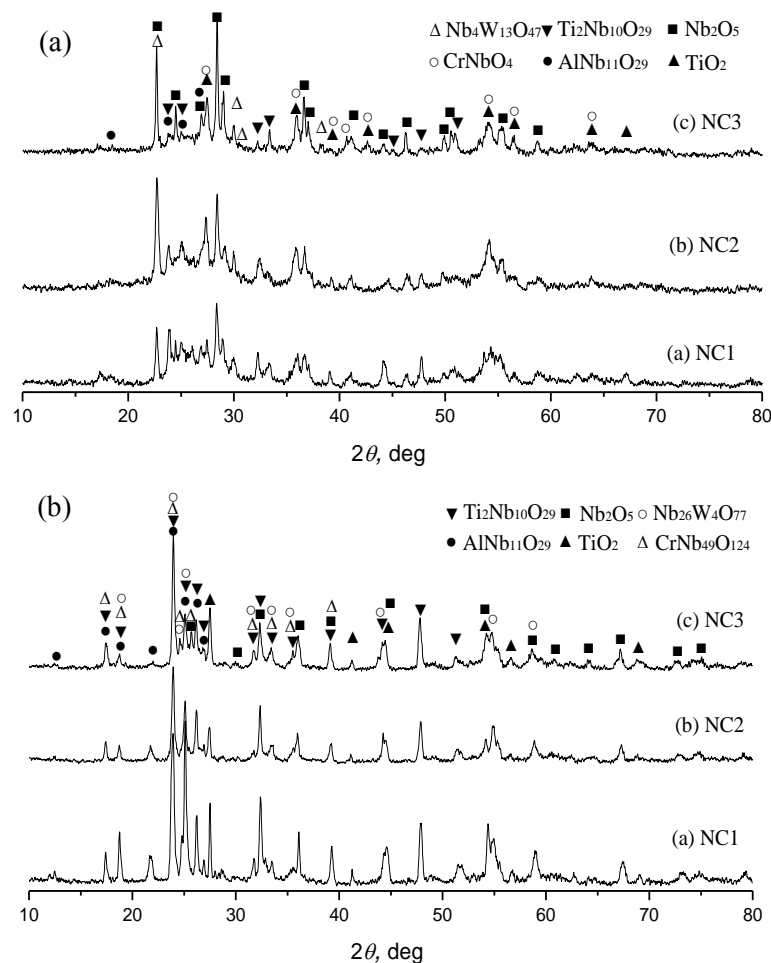


**Figure 7.** XRD patterns of the oxide scales on the samples after oxidation. (a) 800 C; (b) 1100 C.

Figure 6 shows that the sample oxides at  $1100^\circ\text{C}/100\text{h}$ . The particle sizes of the oxides are uniform and have a compact arrangement with some holes, which affects the antioxidant property. The antioxidant properties of the samples at  $1100^\circ\text{C}$  were significantly superior to that at  $800^\circ\text{C}$ . The oxide scales of alloys at  $1100^\circ\text{C}$  are more compact, which reduce the direct contact of oxygen with the base material. Thus, the alloys have good antioxidant properties. According to XRD (Figure 7b), the oxide scales formed on all alloys at  $1100^\circ\text{C}$  contained the  $\text{AlNb}_{11}\text{O}_{29}$ ,  $\text{Ti}_2\text{Nb}_{10}\text{O}_{29}$ ,  $\text{TiO}_2$ ,  $\text{Nb}_{26}\text{W}_4\text{O}_{77}$  and  $\text{Nb}_2\text{O}_5$ . In the NC2 and NC3 alloys, because of the presence of Cr, the  $\text{CrNb}_{49}\text{O}_{124}$  could have also formed. At  $1100^\circ\text{C}$ , the  $\text{Nb}_2\text{O}_5$  oxidation product is reduced, and the oxidation product of other alloy element is increased, therefore, a more dense oxide scale is formed and the oxidation resistance is enhanced.

#### 4. Conclusions

The Nb-20Si-5Al-15Ti-5W-xCr alloys is mainly composed of (Nb, Ti, W)<sub>ss</sub>, Ti,  $\alpha$ -Nb<sub>5</sub>Si<sub>3</sub>, and  $\gamma$ -Nb<sub>5</sub>Si<sub>3</sub> phases and a small amount of (Nb, Ti)<sub>5</sub>Si<sub>3</sub>. At 800°C, the oxide scale is mainly composed of AlNb<sub>11</sub>O<sub>29</sub>, Ti<sub>2</sub>Nb<sub>10</sub>O<sub>29</sub>, TiO<sub>2</sub>, Nb<sub>2</sub>O<sub>5</sub>, Nb<sub>4</sub>W<sub>3</sub>O<sub>47</sub> and Cr<sub>2</sub>Ti<sub>6</sub>O<sub>15</sub>. However, at 1100°C, the oxide scale is mainly composed of AlNb<sub>11</sub>O<sub>29</sub>, Ti<sub>2</sub>Nb<sub>10</sub>O<sub>29</sub>, TiO<sub>2</sub>, Nb<sub>2</sub>O<sub>5</sub> and Cr<sub>2</sub>WO<sub>6</sub>.

Al, Ti and Cr were added to the Nb/Nb<sub>5</sub>Si<sub>3</sub> alloys to obtain dense and integrated oxide scales. In the formed oxide scales, the oxide of Nb was reduced, and the oxides of Al, Ti and Cr were increased. In addition, the compactness of oxide scales and adhesion were improved, which could effectively inhibit the diffusion of oxygen in the composite material, thereby improving the oxidation resistance of the material.

The multi-component alloying of Nb–Si alloys can effectively reduce the rate of high-temperature oxidation. At 800°C with the additions of Al, Ti, W and Cr, the antioxidant properties increased by approximately 10-fold and the “pest” phenomenon was eliminated. Moreover, the oxidation resistance at 1100°C is 5× higher than that at 800°C.

#### Acknowledgements

This work was financially supported by the National Natural Science Foundation of China (Grant Number: 51271091) and the Nature Science Foundation of Jiangxi Province (Project No. 20161BAB206107).

#### References

- [1] Subramanian P R, Mendiratta M G and Dimiduk D M 1996 *JOM* **48**(1): 33–38
- [2] Knittel S, Mathieu S, Portebois L, Vilasi M 2014 *Intermetallics* **47**: 43–52
- [3] Vazquez, Varma SK 2011 *J. Alloy. Compd.* **509** 7027–7033
- [4] Su L, Jia L, Weng J, *et al.* 2014 *Corros. Sci.* **88** 460–465
- [5] Yao D, Zhou C, Yang J, Chen H 2009 *Corros. Sci.* **51** 2619–2627
- [6] Kim WY, Yeo ID, Ra TY, *et al.* 2010 *J. Alloys Compd.* **364** 186–192
- [7] Kang YW, Qu SY, Song JX, *et al.* 2012 *Mater. Sci. Eng. A* **534** 323–328
- [8] Kim WY, Yeo ID, Kim MS, Hanada S 2002 *Mater. Trans.* **43** 3254–3261
- [9] Qu SY, Han YF, Song JX, Kang YW 2007 *Mater. Sci. Forum* **549–549** 1485–1488
- [10] Grammenos I, Tsakiroopoulos P 2010 *Intermetallics* **18** 1524–1530
- [11] Kashyap S, Tiwary CS, Chattopadhyay K 2011 *Intermetallics* **19** 1943–1952
- [12] Zhang SM, Zhou JR, Sha JB 2015 *Intermetallics* **57** 146–155
- [13] Su L F, Jia L N, Jiang K Y, Zhang H 2017 *Int. J. Refract. Met. Hard Mater.* **69** 131–137
- [14] Geng J, Tsakiroopoulos P, Shao G 2007 *Intermetallics* **15** (3): 69–76
- [15] Zelenitsas K, Tsakiroopoulos P 2006 *Mater Sci Eng A* **416**: 269–280
- [16] Geng J, Tsakiroopoulos P, Shao G 2006 *Mater Sci Eng A* **441**: 26–39
- [17] Long W Y, Wang W D, Yao J P 2013 *Applied Mechanics and Materials* **376**: 49–53
- [18] Geng J, Tsakiroopoulos P 2007 *Intermetallics* **15**: 382
- [19] Geng J, Tsakiroopoulos P, Shao G 2007 *Intermetallics* **15**: 270
- [20] Guo J T, Tian Y X, Sheng L Y, Zhou L Z, Ye H Q 2008 *Int J Mat Res* **99**: 1275
- [21] Gale WF, Totemeier TC, editors 2003 *Smithells metals reference book* Oxford: Butterworth-Heinemann p. 4–44
- [22] Zheng H, Lu S, Jianye Z, Guangming L 2009 *Int. J. Refract. Met. Hard Mater.* **27** 659–663
- [23] Pilling NB, Bedworth RE 1923 *J. Inst. Met.* **29** 529–582
- [24] Zheng J, Hou X, Wang X, Meng Y, *et al.* 2015 *Corros. Sci.* **96** 186–195
- [25] Kwai S. Chan 2004 *Metall. Mater. Trans. A* **35A**: 589–597